# ChemComm

Accepted Manuscript


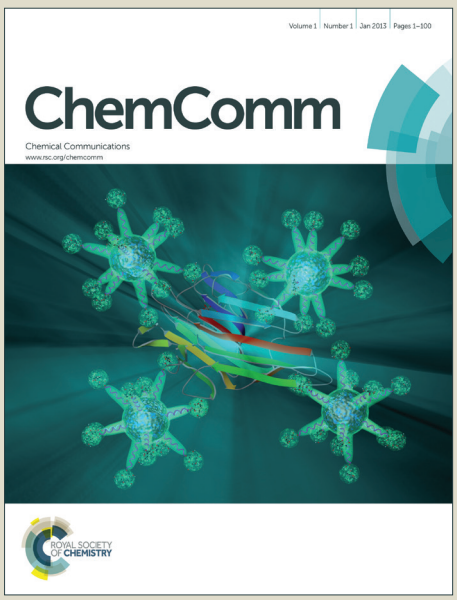





ROYAL SOCIETY OF CHEMISTRY

www.rsc.org/chemcomm

Journal Name

RSCPublishing

COMMUNICATION

# High-performance sodium battery with 9,10-anthraquinone/CMK-3 cathode and ether-based electrolyte

Cite this: DOI: 10.1039/xoxxoooooox

Received ooth January 2012,
Accepted ooth January 2012

DOI: 10.1039/xoxxoooooox

www.rsc.org/

Chunyang Guo[1], Kai Zhang[1], Qing Zhao[1], Longkai Pei[1], and Jun Chen[1,2]*

**We here report much improved electrochemical performance of sodium batteries with the cathode of 9,10-anthraquinone (AQ) encapsulated in CMK-3, ether-based electrolyte of high-concentration $CF_3SO_3Na$ (NaTFS) as sodium salt in triethylene glycol dimethyl ether (TEGDME) solvent, and the anode of Na. The as-prepared micro-nanostructured composite with optimized mass ratio of AQ/CMK-3 = 1:1 delivered an initial discharge capacity of 214 mAh $g^{-1}$ and a capacity retention of 88% after 50 cycles at 0.2C. This means that the combination of AQ/CMK-3 composite cathode and ether-based electrolyte with high-concentration sodium salt is promising in the application of sodium batteries.**

Sodium batteries have gained considerable interest because sodium shows the advantages of high abundance, low cost and similar physic-chemical properties to that of lithium.[1-8] Organic carbonyl compounds such as $Na_2C_8H_4O_4$[9,10], $Na_2C_{10}H_2N_2O_4$[11], $Na_2C_5O_5$[12], $Na_4C_8H_2O_6$[13], $C_{24}H_8O_6$[14] and $Na_2C_6O_6$[15] have recently received attention as electrode materials of sodium batteries owing to their high capacity, structural diversity and eco-friendly synthesis.[16-20] Anthraquinone-based polymers like poly(anthraquinoyl sulfide) (PAQS) displays stable cyclic performance in lithium batteries[21] (210 mAh $g^{-1}$ after 40 cycles at 50 mAh $g^{-1}$) and high rate capability in sodium batteries[22] (130 mAh $g^{-1}$ at 16C and 118 mAh $g^{-1}$ at 32C). As known, 9,10-anthraquinone (AQ, $C_{14}H_8O_2$), which is a typical representation of organic carbonyl compounds as the cathode of lithium batteries, undergoes a reversible two-electron redox reaction during discharge/charge process.[23] Then, one would ask how about using AQ as the electrode material of sodium batteries.

However, the existing problems of carbonyl compounds as the electrode materials of sodium batteries are the poor conductivity and severe capacity fade owing to their high solubility in traditional carbonate-based electrolyte. A main strategy to solve such problems is to prepare electrode composite materials of organic carbonyl compounds and nanostructured carbon.[10,24] In particular, CMK-3, which has large surface area, ordered porous network, large pore volume, good electrical conductivity and low cost, has been used to load organic carbonyl compounds in lithium batteries.[23,25] From this point, encapsulating organic carbonyl compounds in CMK-3 should be interesting for the system of sodium batteries.

On the other hand, electrolyte plays a key role in the battery system. For traditional carbonate-based electrolyte, salt concentration is typically less than 1.2M with the consideration of ionic conductivity, viscosity and dissolubility of the salt. However, the salt concentration of ether-based electrolyte can reach a higher value. Recently, Hu's group proposed a new class of ether-based electrolyte named 'Solvent-in-Salt' with ultrahigh salt concentration for Li-S batteries, which possesses an ionic conductivity of 0.814 mS $cm^{-1}$ and a viscosity of 72 cP at room temperature.[26] It successfully enhances the electrochemical performance of Li-S batteries by inhibiting the dissolution of intermediate lithium polysulphides because salt holds a dominant position in the electrolyte system. Thus, extending this stragety to the system of sodium batteries would be interesting.

Herein, we report the high-performance sodium batteries with the combination of encapsulating AQ in CMK-3 (AQ/CMK-3) as the cathode and adopting ether-based electrolyte with high-concentration $CF_3SO_3Na$ (NaTFS) as sodium salt (in triethylene glycol dimethyl ether (TEGDME) solvent). The detailed preparation of AQ/CMK-3 and ether-based electrolyte with high-concentration NaTFS electrolytes can be seen in supporting information. It was found that AQ/CMK-3 composite with optimized 1:1 mass ratio delivered an initial discharge capacity of 214 mAh $g^{-1}$ and a capacity of 190 mAh $g^{-1}$ (with capacity retention of 88%) after 50 cycles at 0.2C. As comparison, the capacity of pure AQ faded quickly from 178 to 126 mAh $g^{-1}$ (with capacity retention of 71%) after 50 cycles at 0.2C. This study shows that the combination of AQ encapsulated in CMK-3 and ether-based electrolyte with high salt concentration is promising in sodium batteries.

Fig. 1a displays XRD patterns of pure AQ, CMK-3 and the as-prepared composites with selected mass ratios of AQ to CMK-3. The position of all diffraction peaks of AQ match well with the standard XRD pattern of AQ (JCPDS 36-1890) and the strongest peak at 7.7° is assigned to (200) crystal face. XRD pattern of CMK-3 shows a broad peak at 22.7°, which is assigned to (002) crystal face. For lower value of mass ratios of AQ to CMK-3 (1:3, 1:2 and 1:1), there is no obvious diffraction peaks of AQ, which indicates AQ is dispersed well in the nanochannels of CMK-3. When the value of mass ratio of AQ to CMK-3 further increases (2:1 and 3:1),

diffraction peaks of AQ emerge, which demonstrates that excess AQ is dispersed outside the nanochannels of CMK-3. The Raman spectra is shown in Fig. 1b. It is easy to see Raman shifts at 1667, 1600 and 685 $cm^{-1}$, which correspond to C=O of AQ stretching vibration, ring stretching vibration and ring out-of-plane vibration, respectively. Raman spectra of CMK-3 shows two broad peaks at 1607 and 1333 $cm^{-1}$. No characteristic signals of AQ but obvious peaks of CMK-3 can be observed when the mass ratio of AQ/CMK-3 is lower than 1:1. This means that AQ is encapsulated well in CMK-3. On further increasing the amount of AQ, peaks of AQ gradually appear, demonstrating excess AQ is outside of channels of CMK-3. Therefore, the channels of CMK-3 are nearly fully filled when the mass ratio of AQ/CMK-3 reaches 1:1. SEM images in Fig. 1c-d shows that CMK-3 and AQ/CMK-3 are the character of well-ordered nanoscaffolds. After impregnation of AQ, the surface of CMK-3 becomes smooth (Fig. 1d). For comparison, SEM images of AQ/CMK-3 with selected mass ratios of AQ to CMK-3 can be seen in Fig. S1. It is clearly to see that when the value of mass ratio is higher than 1:1, the excess AQ is presented in the form of crystals. Thus, the results suggest that the mass ratio of AQ/CMK-3 = 1:1 is optimum. TEM images also demonstrate the successful impregnation of AQ into mesoporous CMK-3 (Fig. 1e-f). TEM image in Fig. 1e clearly shows the apparent nanochanneled scaffolds of CMK-3. While the confinement of AQ in CMK-3 nanochannels is seen in Fig. 1f. The above results prove that AQ has been successfully encapsulated in CMK-3 nanochanneled scaffolds.

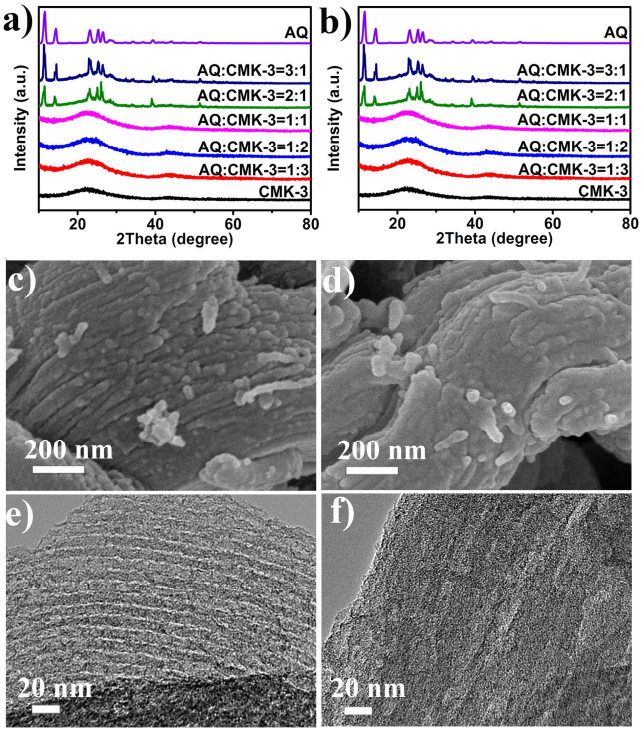


**Fig. 1** Characterization of AQ/CMK-3 nanocomposite: a) XRD patterns and b) Raman spectra of AQ, CMK-3 and AQ/CMK-3 with selected mass ratios of AQ to CMK-3; c) and d) SEM images of CMK-3 and AQ/CMK-3 with the mass ratio of AQ to CMK-3 is 1:1. e) and f) TEM images of CMK-3 and AQ/CMK-3 with the mass ratio of AQ to CMK-3 is 1:1.

Next step, we use electrolyte with high salt concentration to enhance the electrochemical performance of AQ/CMK-3 in sodium battery. $NaPF_6$ and 1,3-Dioxolane (DOL)/ Dimethoxyethane (DME) electrolyte system has been reported for organic sodium battery[23], but the dissolution experiment has proven that the salt concentration cannot reach over 1M (Fig. S2). Therefore, we report a new high salt concentration electrolyte system containing $CF_3SO_3Na$ (NaTFS) as sodium salt and triethylene glycol dimethyl ether (TEGDME) as solvent. Fig. 2a-b displays the molecule structure of NaTFS and TEGDME. In order to investigate the electrolyte system, the physicochemical properties of electrolytes with four different concentrations are tested. Fig. 2c shows the ratios of salt-to-solvent of the electrolyte. In traditional non-aqueous organic electrolytes, the salt concentration usually ranges from 1 to 2M.[26] The salt concentration of this electrolyte is higher than conventional organic electrolytes and can reach a comparatively high value of 4M. In this electrolyte system with high salt concentration, sodium salt plays an important role. Fig. 2d displays Arrhenius plots of the ionic conductivity of the electrolytes with different concentrations over a temperature range from −15 to 55 °C. It can be seen that the ionic conductivity decreases with the increase of salt concentration, but 4M electrolyte still retains a conductivity of 0.79 mS $cm^{-1}$ at 25 °C.

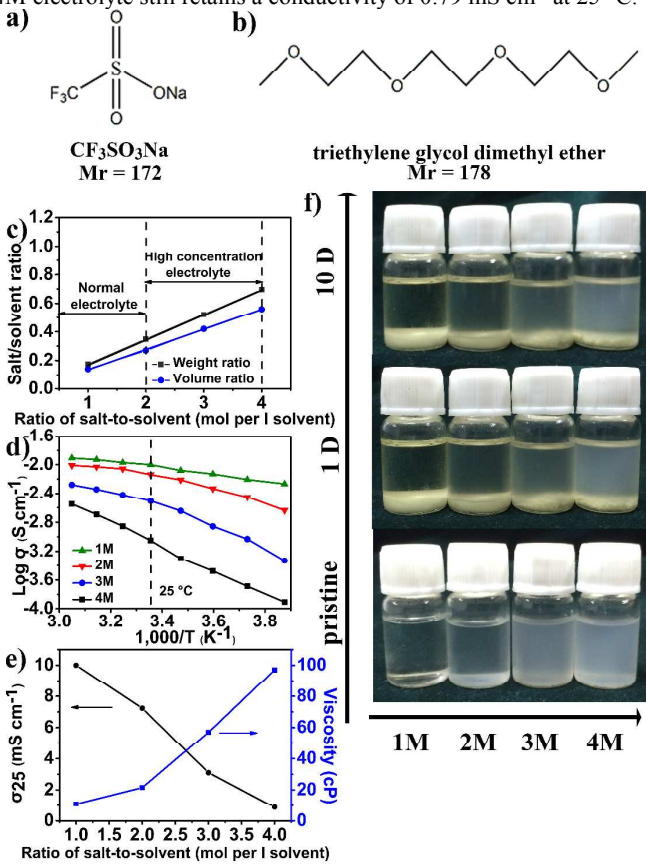


**Fig. 2** Physicochemical properties of high concentration electrolytes: a) Molecule structure of $CF_3SO_3Na$. b) Molecule structure of triethylene glycol dimethyl ether. c) Weight and volume ratio of salt-to-solvent with different ratios of NaTFS to TEGDME. d) Arrhenius plots with different concentrations of the electrolyte (1M: 1 mol $L^{-1}$, 2M: 2 mol $L^{-1}$, 3M: 3 mol $L^{-1}$, 4M: 4 mol $L^{-1}$). e) Viscosity and ionic conductivity of different electrolytes at 25 °C . f) AQ dissolution experiments. 0h: the colour of electrolytes with selected salt concentrations; 1day and 10 day: the colour change of four samples with the same weight of AQ in the electrolytes with different salt concentrations.

Viscosity is another factor to value the electrolyte system. Fig. 2e shows the plot of viscosity of electrolytes with different concentrations at 25 °C. 4M electrolyte reaches a high viscosity of 97 cP. Previous report shows in the electrolyte system with ultrahigh salt concentration and high viscosity, when solvated cations are decreased, large anions are more seriously dragged than the small unsolvated cations.[26] Similarly, in the present electrolyte system with high salt concentration, the number of solvated sodium ions

decreases and large $TFS^-$ anions move far slower than small unsolvated sodium cations. Therefore, compared with low salt concentration electrolytes, the mobility of unsolvated sodium cations is much easier in electrolyte with high salt concentration. To further confirm whether this high salt concentration electrolyte depresses the dissolution of AQ, we performed AQ dissolution experiments in electrolytes with different salt concentrations (Fig. 2f). In the system of 1 to 3M electrolytes with lower salt concentration, yellow colour is seen after 1 day, meaning that AQ is dissolved. However, in 4M electrolytes with high salt concentration, the colour is nearly unchanged even after 10 days. This shows that 4M electrolyte with high salt concentration is very effective in depressing the dissolution of AQ in the electrolyte.

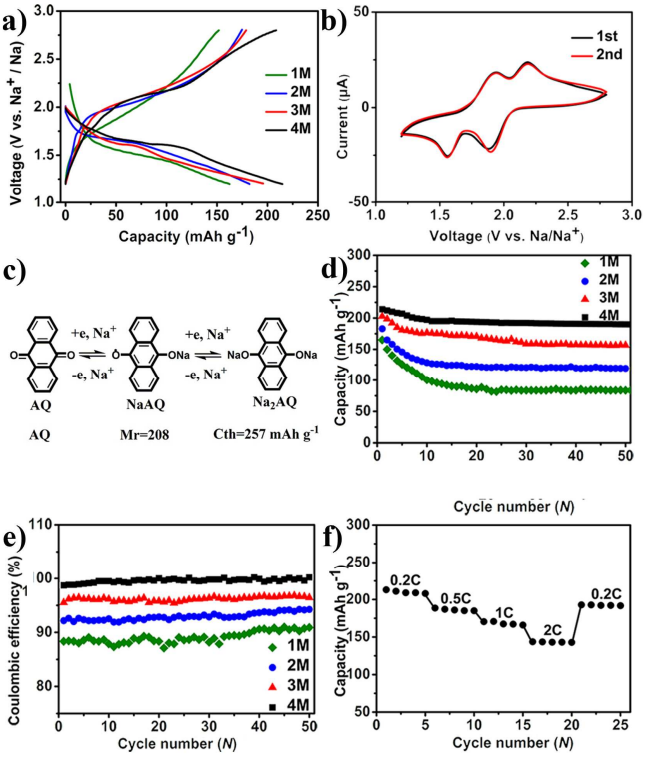


**Fig. 3** Electrochemical performance of AQ/CMK-3 in sodium battery: a) First discharge-charge curves of AQ/CMK-3 electrodes in electrolytes with different concentrations at 0.2C. b) CV curves of AQ/CMK-3 in 4M electrolyte. c) Mechanism of AQ during charge/discharge process. d) Cyclic performance. e) Coulombic efficiency at a current rate of 0.2C (coulombic efficiency = charge capacity/ discharge capacity). f) Rate capability with 4M electrolyte.

To investigate the effectiveness of different concentrations electrolytes, electrochemical performance of AQ/CMK-3 is displayed in Fig. 3. As comparison, electrochemical performance of AQ in the electrolytes with different salt concentrations is exhibited in Fig. S3. As shown in Fig. 3a, with the increase of salt concentration in the electrolyte, the initial discharge capacity of AQ/CMK-3 increases. Among four different electrolytes, AQ/CMK-3 in 4M electrolyte delivers the highest initial discharge capacity of 214 mAh $g^{-1}$ and charge capacity of 208 mAh $g^{-1}$ at 0.2C. In addition, the initial discharge capacity of AQ/CMK-3 is always higher than AQ in different concentrated electrolyte (Fig. S3a), demonstrating that CMK-3 confinement enhances the utilization of carbonyl functional groups. Fig. 3b shows CV curves of AQ/CMK-3 in 4M NaTFS/TEGDME electrolyte. The four well-defined peaks can be observed at 1.89, 1.57, 1.92 and 2.18V (Fig. 3c). The results demonstrate a two-electron redox reaction of AQ during discharge/charge process (Fig. 3c). AQ/CMK-3 also presents a better cycling performance in 4M electrolyte than that in other electrolytes with lower salt concentrations. Even after 50 cycles, AQ/CMK-3 still remains a reversible capacity of 190 mAh $g^{-1}$ with a high capacity retention of 88% (Fig. 3d). Fig. 3e displays coulombic efficiency of AQ/CMK-3 in electrolyte with the concentration range from 1M to 4M. In low sodium salt concentration electrolyte, the coulombic efficiency is so low, which is due to that the dissolution of AQ/CMK-3 is serious. Compared with low concentration sodium salt electrolyte, 4M electrolyte makes it reach nearly 100% coulombic efficiency after 5 cycles. This means that the dissolution of AQ is effectively reduced. In Fig. 3f , AQ/CMK-3 shows good rate performance in 4M electrolyte. It can achieve capacities of 208, 185, 166 and 143 mAh $g^{-1}$ at 0.2, 0.5, 1 and 2C, respectively. After 20 cycles, when the current rate returns to 0.2C, a reversible capacity of 192 mAh $g^{-1}$ maintains.

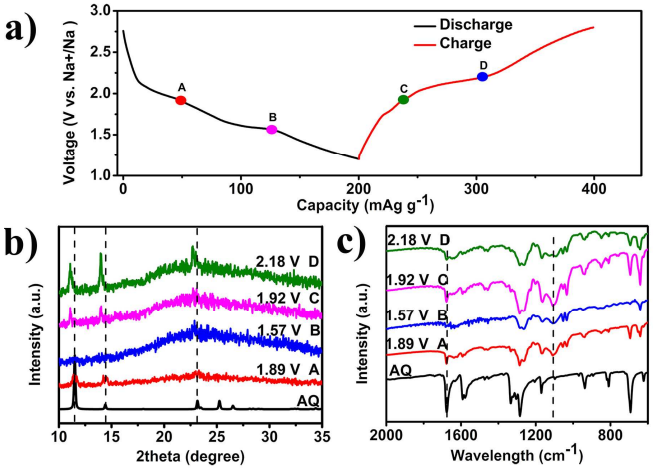


**Fig. 4** Structural evolution of AQ/CMK-3 in the full potential window of 1.2—2.8V: a) A potential-capacity profile at 0.1C rate. b) Ex situ XRD for products taken at different states. c) Ex situ IR for products taken at different states.

This reversible electrochemical reactions are also confirmed by structural evolution of AQ/CMK-3 in the full potential window of 1.2−2.8 V (Fig. 4). Lower current rate (0.1C) was applied to test discharge and charge profiles. Fig. 4a shows discharge and charge curves of AQ/CMK-3 with 4M electrolyte at a current rate of 0.1C. All the CV peak potentials (Fig. 3b) are exactly consistent with the four well-defined potential plateaus in the discharge/charge curves in Fig. 4a. Fig. 4b exhibits XRD patterns of AQ and the products taken at different plateaus. As the discharge potential decreases, diffraction peaks of AQ gradually disappear. The diffraction peaks of AQ gradually emerge again when the charge potential increases. This trend is identical to the conclusion drawn from IR spectra. As shown in Fig. 4c, strong vibrations center at 1680 and 1100 $cm^{-1}$ are ascribed to C=O stretching mode of carboxylate groups and the =C-O stretching mode of enolate groups of AQ, respectively. As discharged to 1.89 V (A), it shows signals of both C=O and =C-O. This means that one of C=O groups of AQ has changed to =C-O group because the C=O of AQ undergoes one electron reduction during the first step of discharge process. When fully discharged to 1.57 V (B), the C=O signal disappears, while the =C-O remains. This indicates that the other C=O group gains one electron. For the charge process, its similar result with oxidation process is obtained.
Fig. S4a and S4b display the Nyquist plots of AQ and AQ/CMK-3 electrodes in 4M electrolyte at 1.89 V discharge state. Experimental profiles of the two electrodes consist of a high-medium frequency semicircle and a low frequency inclined line. The semicircle is assigned to the combination of charge transfer and surface film

resistances. The charge transfer resistances ($R_{ct}$) of AQ electrode decreases from 1150 Ω at 293 K to 290 Ω at 323 K, while AQ/CMK-3 shows $R_{ct.}$ of 801 Ω at 293 K and 260 Ω at 323 K. Fig. S4c shows the Arrhenius plots of ln($T$/$Rct$) versus $1/T$, from which the activation energy $E_a$ is calculated to be 37.9 kJ mol$^{-1}$ for AQ and 30.5 kJ mol$^{-1}$ for AQ/CMK-3, respectively. In comparison, the EIS profiles of AQ and AQ/CMK-3 electrodes at 1.57 V state (Fig. S5) also show similar result. The much lower $R_{ct}$ of AQ/CMK-3 electrode indicates faster charge-transfer process and higher electrical conductivity. At either 1.89 V or 1.57 V discharge state, the activation energy of AQ/CMK-3 is lower than that of AQ. This indicates that sodium intercalation kinetics of AQ/CMK-3 is more facile. The enhanced kinetics arises from the structure of the AQ/CMK-3 nanocomposites, in which the CMK-3 provides a high electronic and ionic conductivity. This contributes to the better rate capability.

All the above results mean that AQ is confined into CMK-3 to reduce its dissolution and thus shows better rate performance and cycling performance. Furthermore, the whole electrolyte system can be considered to be a sodium salt with a high concentration of saturation.[26] Therefore, AQ is hard to dissolve into the given electrolyte, showing much enhanced electrochemical performance. Though the cycling stability and rate performance is not as good as anthraquinone based polymers', which is attributed to that the polymer phase with thioether bridge bond is insoluble in the electrolyte and more stable than AQ, AQ/CMK-3 with high salt concentration electrolyte is much easier to prepare. This new method would overcome the dissolution problem of organic electrode in the electrolyte. It is noted that future studies would focus on increasing the tap density of the organic materials, finding anode materials to match with AQ cathode with higher voltage of the battery system, and improving the volumetric energy density of the full batteries.

In summary, the combination of AQ/CMK-3 composite cathode and ether-based electrolyte with high concentration of $CF_3SO_3Na$ (NaTFS) as sodium salt and triethylene glycol dimethyl ether (TEGDME) as solvent is effective to obtain much improved electrochemical performance. In particular, an optimization of AQ/CMK-3 (with 50 wt% AQ) in 4M high salt concentration electrolyte exhibits an initial capacity of 214 mAh g$^{-1}$ and 190 mAh g$^{-1}$ (a capacity retention of 88%) after 50 cycles at 0.2C. This strategy not only protects the organic carbonyl materials from dissolving into the electrolyte, but also boosts the ion diffusion in the electrolyte and electrical conductivity of the cathode. This work enlightens the application of inorganic-organic nanocomposite and high salt concentration electrolyte in sodium batteries,.

## Acknowledgements

This study was supported by the Programs of National 973 (2011CB935900), NSFC (51231003), MOE (113016A, B12015 and IRT13R30), and Tianjin Project (13JCQNJC06400).

## Notes and references

[1]*Key Laboratory of Advanced Energy Materials Chemistry (Ministry of Education) and* [2]*Collaborative Innovation Center of Chemical Science and Engineering, Nankai University, Tianjin, 300071, People's Republic of China. E-mail: chenabc@nankai.edu.cn; Tel/Fax: +86-22-23506806.*

† Electronic Supplementary Information (ESI) available: Test measurement of prepared materials, SEM images of AQ/CMK-3 with selected mass ratios of AQ to CMK-3 , $NaPF_6$ dissolution experiment and electrochemical performance AQ and AQ/CMK-3 in sodium battery. See DOI: 10.1039/c000000x/

1. A. Powell, Z. Stoeva, J. Lord, R. Smith, D. Gregory and J. Titman, *Phys.Chem. Chem. Phys.*, 2013, 15, 816-823.
2. Q. Wang, A. Madsen, J. Owenb and M. Weller, *Chem. Commun.*, 2013, 49, 2121-2123.
3. J. Song, Z. Yu, M. Gordin, S. Hu, R. Yi, D. Tang, T. Walter, M. Regula, D. Choi, X. Li, A. Maniyannan and D. Wang, *Nano Lett.*, 2014, 14, 6329-6335.
4. K. Sakaushi, E. Hosono, G. Nickerl, T. Gemming, H. Zhou, S. Kaskel and J. Eckert, *Nat. Commun.*, 2012, 4, 1485.
5. K. Zhang, Z. Hu, Z. Tao and J. Chen, *Sci. China Mater.*, 2014, 57, 42–58.
6. W. Li, S. Chou, J. Wang, H. Liu and S. Dou, *Nano Lett.*, 2013, 13, 5480−5484.
7. L. Pei, Q. Jin, Z. Zhu, Q. Zhao, J. Liang and J. Chen, *Nano Res.*, 2015, 8, 184–192.
8. K. Zhang, X. Han, Z. Hu, X. Zhang, Z. Tao and J. Chen, *Chem. Soc. Rev.*, 2015, 44, 699–728.
9. Y. Park, D. Shin; S.Woo, N. Choi, K. Shin, S. Oh, K. Lee and S. Hong, *Adv. Mater.*, 2012, 24, 3562-3567.
10. L. Zhao; J. Zhao; Y. Hu, H. Li, Z. Zhou; M. Armand and L. Chen, *Adv. Energy Mater.*, 2012, 2, 962-965.
11. S. Renault, V. Mihali, K. Edström and D. Brandell, *Electrochem. Commun.* , 2014, 45, 52-55.
12. C. Luo, R. Huang, R. Kevorkyants, M. Pavanello, H. He and C. Wang, *Nano Lett.*, 2014, 14, 1596-1602.
13. S. Wang, L. Wang, Z. Zhu, Z. Hu, Q. Zhao, and J. Chen, *Angew. Chem. Int. Ed.*, 2014, 53, 5892-5896.
14. W. Luo , M. Allen , V. Raju and X. Ji , *Adv. Energy Mater.*, 2014, 1400554.
15. K. Chihara, N. Chujo, A. Kitajou and S. Okada, *Electrochim. Acta* 2013, 110, 240-246.
16. Y. Liang, Z. Tao and J. Chen, *Adv. Energy Mater.*, 2012, 2, 742-769.
17. Y. Hanyu, Y. Ganbe and I. Honma, *J. Power Sources*, 2013, 221, 186- 190.
18. Z. Song, T. Xu, M. Gordin, Y. Jiang, I. Bae, Q. Xiao, H. Zhan, J. Liu and D. Wang, *Nano Lett*., 2012, 12, 2205-2211.
19. Z. Song, H. Zhan and Y. Zhou, *Angew. Chem. Int. Ed.* , 49, 8444-8448.
20. Z. Zhu, H. Li, J. Liang, Z. Tao and J. Chen, *Chem. Commun.*, 2015, 51, 1446-1448.
21. Z. Song, H. Zhan and Y. Zhou, *Chem. Commun.*, 2009, 448-450.
22. W. Deng, X. Liang, X. Wu, J. Qian, Y. Cao, X. Ai, J. Feng and H. X. Yang, *Sci. Rep.*, 2013, 3, 2671.
23. L. Zhao, W. Wang, A .Wang, Z.Yu, S.Chen and Y.Yang, *J. Electrochem. Soc.*, 2011, 158, A991-A996.
24. C. Luo, Y. Zhu, Y. Xu, Y. Liu, T. Gao, J. Wang, C. Wang, *J. Power Sources*, 2014, 250, 372-378.
25. H. Li, W. Duan, Q. Zhao, F. Cheng, J. Liang and J. Chen, *Inorg. Chem. Front.*, 2014, 1, 193-199.
26. L. Suo, Y. Hu, H. Li, M. Armand and L. Chen, *Nat. Commun*., 2013, 4, 1481.



 